Chemical Engineering Journal 453 (2023) 139716

Contents lists available at ScienceDirect

Chemical Engineering Journal

journal homepage: www.elsevier.com/locate/cej

Waterproof conductive fiber with microcracked synergistic conductive layer for high-performance tunable wearable strain sensor

Shiyin Yang [a,1], Wenke Yang [a,1], Rui Yin [b], Hu Liu [a,*], Hongling Sun [a], Caofeng Pan [c], Chuntai Liu [a], Changyu Shen [a]

[a] Key Laboratory of Materials Processing and Mold (Zhengzhou University), Ministry of Education, National Engineering Research Center for Advanced Polymer Processing Technology, Zhengzhou University, Zhengzhou, Henan 450002, China
[b] China Astronaut Research and Training Center, Beijing 100094, China
[c] Beijing Institute of Nanoenergy and Nanosystems, Chinese Academy of Sciences, National Center for Nanoscience and Technology (NCNST), Beijing 100083, China

ARTICLE INFO

Keywords:
Strain sensor
Microcrack
Synergistic conductive network
Tunable sensing performance
Waterproof

ABSTRACT

With the rapid development of wearable smart electronic devices, flexible strain sensors with high sensitivity in a wide working range are urgently demanded. Meanwhile, good self-cleaning and anti-corrosion properties are also essential for daily use. Herein, a waterproof conductive spandex fiber strain sensor with microcracked synergistic Ag nanoparticles (AgNPs)-carbon nanotubes CNTs conductive layer was designed and fabricated *via* the solvent swelling, non-solvent-induced phase separation (NIPS), and low surface energy treatment process. Benefiting from the stable synergistic conductive network and the ultrasensitive microcrack structure, the sensor exhibits excellent overall strain sensing performances, including high sensitivity (gauge factor is 48,310 within 335–400% strain), wide working range (0–400%), ultralow detection limit (0.1%), fast response/recovery time (80 ms/100 ms), and long-term fatigue resistance over 10,000 cycles, making it reliably and precisely distinguish both violent human movements and subtle physiological signals. More importantly, strain sensing range and sensitivity of the sensor can also be effectively tunned through changing the AgNPs loading in the synergistic conductive network, enabling it to be applicable for different application scenarios. What's more, the waterproof surface with good self-cleaning and anti-corrosion properties also endows the sensor with great potential for real-time body motion monitoring under humid and underwater environments without being interfered. This study provides a facile one-step method for the fabrication high-performance flexible strain sensor.

1. Introduction

With the rapid development of wearable smart electronic devices, flexible strain sensors as the core component have attracted enormous attentions. Compared with traditional rigid metal based strain sensors, conductive polymer composites (CPCs) based strain sensors possess the incomparable advantages in flexibility, bending resistance, and stretchability, showing great potential in the fields of human motion monitoring [1,2], remote medical diagnostics [3,4], and human–machine interface [5,6]. Generally, high sensitivity and wide working range are two important factors need to be considered for the design of strain sensors. For CPCs based flexible strain sensors, high sensitivity means the significant interruption of conductive path under subtle strain change, while the wide working range requires the stable effective conductive network during a wide strain range [7,8]. Hence, CPCs based flexible strain sensors with high sensitivity in a wide working range to achieve highly sensitive detection of both large and small strain is still a great challenge.

Benefiting from the open of microcracked conductive layer induced significant resistance variation, the construction of microcrack structure has been widely applied and verified to be an effective strategy to improve the sensitivity of the sensor specifically for the subtle deformation [9–13]. However, the separation of microcrack can usually lead to the complete destruction of whole conductive network quickly, causing the limited sensing range. To solve this problem, our group has successfully achieved the controllable construction of microcrack structure with different microcrack densities, which effectively extends the sensing range while maintaining a high sensitivity in the whole

* Corresponding author.
E-mail address: liuhu@zzu.edu.cn (H. Liu).
[1] These authors contributed equally to this work.

https://doi.org/10.1016/j.cej.2022.139716
Received 10 August 2022; Received in revised form 25 September 2022; Accepted 6 October 2022
Available online 12 October 2022

sensing range [14,15]. In fact, according to be previous reported works, the sensing range of strain sensor can be easily improved based on the synergistic effect in the conductive network with different dimensional conductive fillers [16,17] and the construction of specifical structures (i.e., wave-like structure [18,19], spiral structure [20–22], and serpentine structure [23,24]), which deform with the applied strain without destroying the conductive network seriously. So, the combination of microcrack structure with them to construct the synergistic conductive network will undoubtly be a promising strategy.

Furthermore, as a wearable strain sensor, a good self-cleaning and anti-corrosion is essential due to the inevitable exposure to humid air, sweat, acid, alkali, and other liquids in daily use, which can seriously affect the sensing performance and service life of sensor. The simple and effective way to improve the corrosion resistance is to make a hydrophobic treatment of sensor surface, where the hydrophobic surface can repel water droplets effectively, thus preventing the aqueous solutions from diffusing into the interior to interfere the sensor [25–28]. Recently, the introduction of additional superhydrophobic SiO_2 layer has been widely adopted to obtain the waterproof sensors [29–31], but its interfacial adhesion with the strain sensitive layer is still a key problem that affects the stability of sensor during the daily use. In addition, the complicated multi-step processing technique also need effective but simple modification methods to achieve the desired waterproofness.

Herein, conductive spandex fiber was fabricated *via* the simple solvent swelling and non-solvent-induced phase separation (NIPS) process, during which the synergistic Ag nanoparticles (AgNPs)-carbon nanotubes (CNTs) conductive layer with ultrasensitive microcrack structure was successfully constructed. After that, low surface energy 1H,1H,2H,2H-Perfluorodecanethiol (PFDT) was applied to modify the outer AgNPs aggregation to obtain the desired waterproof strain sensor without complex hydrophobic treatment. Here, the effect of AgNPs loading in the synergistic conductive network on the strain sensing was systematically investigated, and tunable strain sensing and sensitivity were easily achieved for the prepared sensor. Besides, the synergistic effect between 0 dimensional AgNPs and one dimensional CNTs and the constructed microcrack structure endow the sensor with excellent overall strain sensing performances, including high sensitivity (gauge factor is 48,310 within 335–400% strain), wide working range (0–400%), ultralow detection limit (0.1%), fast response/recovery time (80 ms/100 ms), and long-term fatigue resistance over 10,000 cycles. As a result, the sensor can be applied for the detection of different human movements (i.e., finger bending, wrist flexing, and walking) and physiological signals (i.e., respiration, and facial muscle). Importantly, the constructed waterproof surface with good corrosion resistance and self-cleaning properties can also makes the sensor have great promising application in humid and underwater environments.

2. Experimental

2.1. Materials and chemicals

Silver trifluoroacetate (STA, $AgCF_3COO$, 98%) was purchased from Beijing Innochem Science & Technology Co., ltd., China. 1H,1H,2H,2H-Perfluorodecanethiol (PFDT, 97%) was acquired from Shanghai Aladdin Biochemical Technology Co., ltd., China. Spandex fiber (SF) was purchased from Haining Kaiwei Textile Co., ltd., China. Carbon nanotubes (CNTs) were bought from Zhongke Time Nano Co., ltd. Tetrahydrofuran (THF), hydrazine hydrate ($N_2H_4{\cdot}H_2O$, 80%), and ethanol were purchased from Tianjin Fuyu Fine Chemical Co. ltd., China. Tris (hydroxymethyl) aminomethane hydrochloride (Tris-HCl) and dopamine (DA) were acquired from Shanghai Macklin Biochemical Co., ltd. All the chemicals and materials are used as received without further treatment.

2.2. Preparation of waterproof conductive fiber

Specifically, 0.1 g Tris-HCl power and 28 mg DA were first dissolved in 20 mL deionized (DI) water to prepare the DA/Tris-HCl buffer solution (1.4 mg/mL, pH = 8.5), and the original SF was immersed for 12 h at room temperature under magnetic stirring to obtain the polydopamine (PDA) coated SF (*p*-SF), which was then rinsed in DI water for several times to remove the unreacted chemicals and dried in an oven at 60 ℃ for 1 h. After that, homogeneous STA/CNTs/THF dispersion was prepared by dispersing CNTs into the well solved STA/THF solution under ultrasonication for 20 min. Here, CNTs concentration was fixed to be 4 mg/mL, and series of different STA concentrations (0.1, 0.3, 0.5 mol/mL) were configured. Subsequently, the prepared *p*-SF was dipped into the obtained STA/CNT/THF dispersion for 20 min, followed by transferring to the diluted hydrazine hydrate aqueous solution (20 wt%) for 5 h to reduce STA to Ag nanoparticles (AgNPs). After rinsing in DI water and drying in an oven at 60 ℃ for 1 h, the obtained AgNPs/CNTs@*p*-SF (AgC@*p*-SF) was further treated in PFDT/ethanol solution (0.02 wt%) for 50 min, washed with DI water and dried in an oven at 60℃ for 2 h, obtaining the designed PFDT/AgNPs/CNTs@*p*-SF (FAgC@*p*-SF) waterproof conductive fiber. In this study, FAgC@*p*-SF using a STA concentration of × was denoted as FAgC@*p*-SF-*x*. Besides, CNTs@*p*-SF (C@*p*-SF) and PFDT/CNTs@*p*-SF (FC@*p*-SF) were also fabricated for comparation.

2.3. Characterization

Scanning electron microscopy (SEM) was performed on a JEOL JSM7500F instrument at an accelerating voltage of 5 kV to observe the sample's surface morphology. X-ray diffractometer (XRD, D8 Advance, Bruker AXS, German) with monochromatic Cu Ka radiation (λ = 1.54 Å) was used to characterize the crystal structure of sample with a scanning rate of 10° min^{-1}. The molecular structure of sample was analyzed by Raman spectroscopy (DXR, GX-PT-2412, Thermo, Waltham, MA, USA) with a 532 nm laser. Surface chemical composition of sample was detected using an X-ray photoelectron spectrometer (XPS, Thermo ESCALAB 250XI) with an excitation source of Al Kα radiation. Fibers are tightly wound round a plat sheet (Fig. S1) for water contact angle (WCA) testing using an optical CA measuring equipment (SL200KS), and measurements of five different positions were averaged. In this study, conductive tape was applied as flexible electrodes to connect with the two ends of the obtained conductive fiber with a length of 20 mm for the fabrication of flexible strain sensor. Tensile strain sensing performance of the sensor was investigated by using a digital multimeter and a universal tensile tester (UTM2203, load cell = 100 N, Shenzhen Suns Technology Stock Co. ltd., China) to in-situ record the resistance change.

3. Results and discussion

Fig. 1a shows the schematic diagram for the preparation of FAgC@*p*-SF waterproof conductive fiber (the details are listed in the experimental part), which mainly involves the construction of microcracked synergistic conductive layer and surface hydrophobic treatment. Commercial SF with excellent elasticity and stretchability was chosen as the matrix and treated in DA solution, where the SF turns from white to gray-brown after the self-polymerization of PDA and its diameter keeps almost unchanged (Fig. 1b&b′). Then, solvent swelling technology was applied to enable the CNTs and STA in THF solution to transfer into the substrate surface. Meanwhile, the unsaturated/aromatic hydrocarbons and hydroxyl groups (–OH) of the self-polymerized PDA layer can also react with Ag^+ and the trifluoroacetate anions ($CF_3COO^-_2$) of STA, respectively, promoting the adsorption of Ag precursor on the surface significantly. After being transferred to the hydrazine solution, the reduction of Ag^+ into AgNPs and the non-solvent-induced phase separation (NIPS) where the mass exchange between the THF and water proceed simultaneously. During this process, CNTs and AgNPs are wrapped by the phase separated SF matrix, constructing the stable synergistic CNTs-AgNPs conductive network. Meanwhile, the PDA absorbed Ag^+ is also beneficial for the formation of AgNPs aggregation layer on the fiber

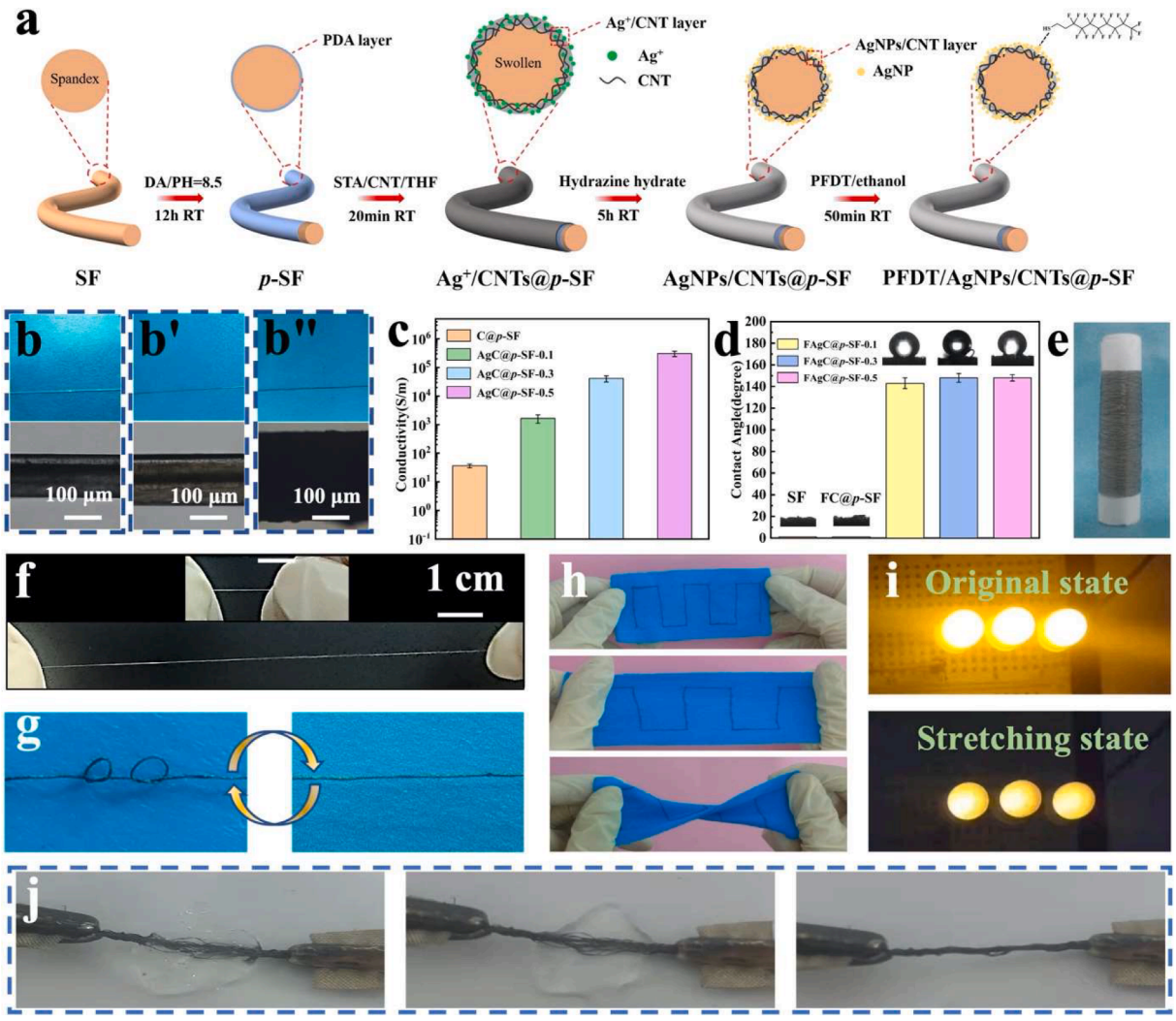

Fig. 1. Preparation process and characterization of FAgC@*p*-SF waterproof conductive fiber. (a) Schematic diagram for the preparation of waterproof conductive fiber. Digital photos and polarized optical microscopy of (b) SF, (b′) *p*-SF, and (b″) AgC@*p*-SF. (c) Conductivity and (d) WCA of SF and different waterproof conductive fibers. (e) A batch of waterproof conductive fiber with a length of 100 m. Digital photos showing the excellent (f) stretchability, (g) knotability, and (h) stitchability of the resultant waterproof conductive fiber. (i) Stretching induced brightness change of LED connected with the waterproof conductive fiber.

surface, which can easily evolve into the ultrasensitive microcrack structure upon external tension [32]. Obviously, as shown in Fig. 1b″, the resultant AgC@*p*-SF exhibits a silver-grey color, and the diameter of fiber also exhibits an obvious increase from 107 μm to 181 μm due to the existence of CNTs-AgNPs conductive layer. Here, as seen in Fig. 1c, the electrical performance of the AgC@*p*-SF can be effectively tunned through changing the STA concentrations, and the electrical conductivity is significantly improved from 36.5 S/m for C@*p*-SF to 304,429 S/m for AgC@*p*-SF-0.5, which can be explained by the fact that more perfect conductive network is constructed with the help of denser reduced AgNPs and its synergistic effect with CNTs.

After that, PFDT molecules was further introduced onto the conductive layer through a dip-coating process, aiming to achieve a hydrophobic surface based on the combination of fluorine-containing molecules and microstructured AgNPs cluster. Obviously, as illustrated in Fig. 1d, in comparation with the pristine SF with a WCA of 0°, all the prepared FAgC@*p*-SF possess a WCA higher than 140°, and a higher STA concentration is also beneficial for larger WCA, indicating that the hydrophobicity of fiber surface is effectively improved. But it should be noted that the FC@*p*-SF also maintains the hydrophilicity of pristine SF, demonstrating the importance of AgNPs for the construction of hydrophobic surface. Here, the facilely solvent swelling, reduction/NIPS, and dip-coating process afford great promise for scale production, and a 100 m FAgC@*p*-SF waterproof conductive fiber can be easily collected (Fig. 1e), which can be stretched to a strain up to 600% without being broken (Fig. 1f). Importantly, it can also be knotted repeatedly (Fig. 1g) and integrated into flexible fabrics through the normal sewing method with good adaptability to different mechanical deformation such as stretching and twisting (Fig. 1h), enabling it to be appliable for wearable flexible electronics. In a designed electrical circuit using the prepared waterproof conductive fiber as a wire (Fig. 1i), the light intensity of the connected LED turns to be weaker and recovers to its initial state upon cyclic stretching and releasing the fiber (Video S1), demonstrating the great potential of our prepared waterproof conductive fiber to serve as an ideal strain sensor.

Surface morphologies of different waterproof conductive fibers were systematically investigated. Compared with the glossy surface of original SF (Fig. S2), FC@*p*-SF exhibits a wrinkled rough surface with amounts of bulges due to phase separation of SF matrix from THF during the reduction process, and the entangled CNTs are also partially embedded into the SF surface based on the swelling effect (Fig. 2a&e). As for the FAgC@*p*-SF with a lower STA loading, it can be clearly observed from Fig. 2b&f that the reduced AgNPs with a diameter of 70 nm are distributed on the wrinkled surface, where some AgNPs are connected with the embedded CNTs and other form obvious aggregation with the entangled CNTs outside the SF surface, demonstrating the

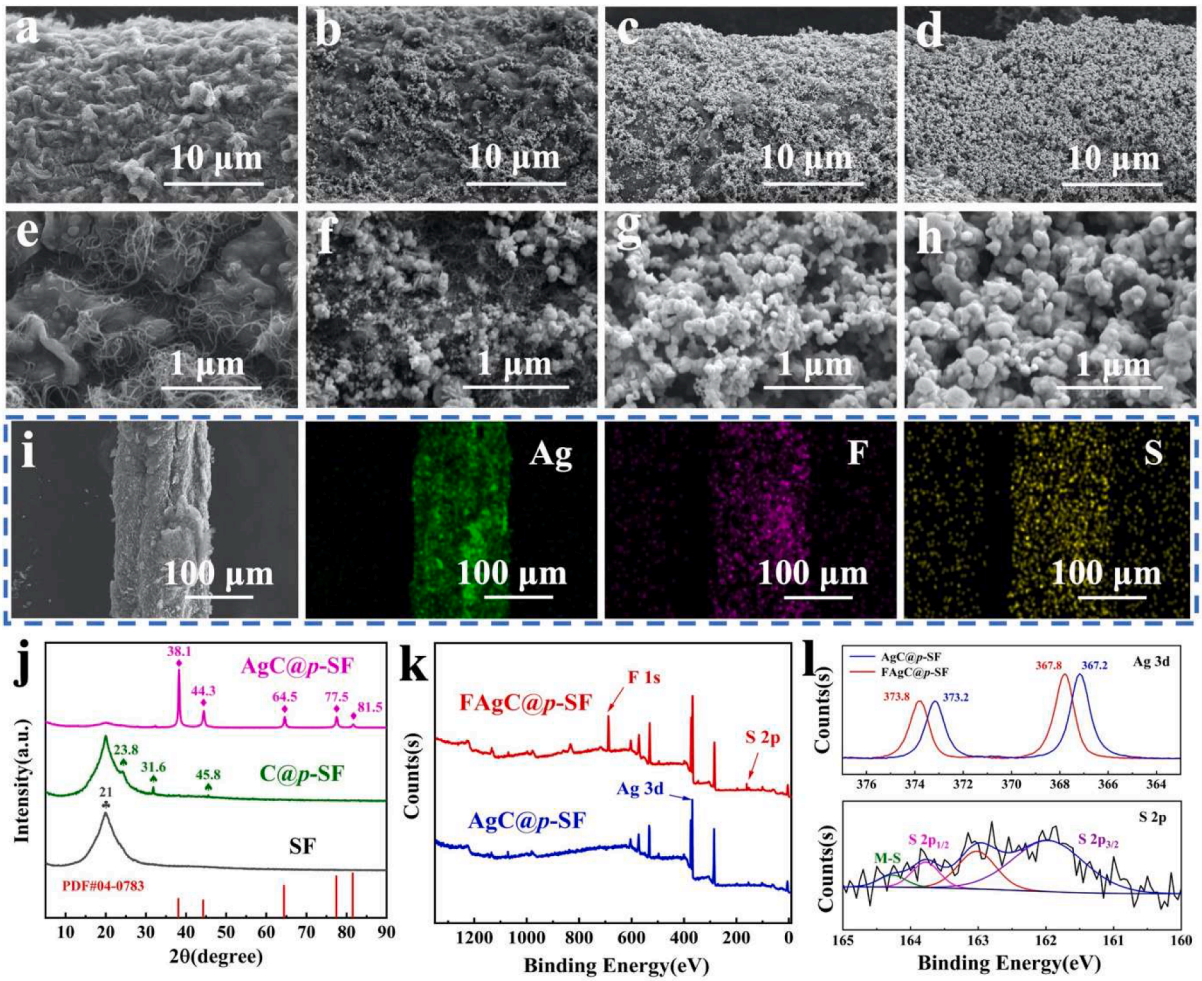

Fig. 2. SEM images of (a, e) FC@*p*-SF, (b, f) FAgC@*p*-SF-0.1, (c, g) FAgC@*p*-SF-0.3, (d, h) FAgC@*p*-SF-0.5. (i) SEM image of FAgC@*p*-SF-0.3 with the corresponding EDS mapping images of Ag, F, and S elements. (j) XRD spectra of SF, C@*p*-SF, and AgC@ *p*-SF. (k) XPS spectra and (l) high-resolution Ag 3d and S 2p.

successful construction of the designed synergistic conductive network. With the further increase of STA loading in the THF solution, the whole surface of FAgC@*p*-SF turns to be completely covered by AgNPs (Fig. 2c&d). Besides, as shown in Fig. 2g&h, the AgNPs aggregation presents the special micro/nano architecture that affects the final hydrophobicity of the fiber significantly. Fig. 2i display the energy dispersive X-ray spectrometer (EDS) mapping images of different elements of FAgC@*p*-SF-0.3, where the Ag element (from Ag conductive layer) and F/S elements (from PFDT) are homogeneously distributed over the entire fiber, ensuring the stable electrical and hydrophobic properties.

After that, XRD pattern were conducted to identify the successful introduction of CNTs and AgNPs. As shown in Fig. 2j, a broad diffraction peak ranging from 12° to 30° exists in the XRD pattern of original SF, which is mainly ascribed to the crystal plane of the hard segment of spandex. Additional three micro-peaks of 23.8, 31.6, and 45.8 corresponding to the 002, 111, 220 crystal planes of CNTs appear for C@*p*-SF [33], and another five sharp diffraction peaks at 38.1°, 44.3°, 64.5°, 77.5°, and 81.5° that are assigned to the 111, 200, 220, 311, and 222 crystal planes of AgNPs are also clearly observed for AgC@*p*-SF. The surface chemical composition was further analyzed using XPS to verify the PTDT modification and its interaction with AgNPs. For the survey spectrum of AgC@*p*-SF shown in Fig. 2k, the additional Ag 3d peak (367.8 eV) is observed except for the C 1 s (284.8 eV) and O 1 s (532.8 eV) of original SF (Fig. S3), demonstrating the existence of AgNPs. Then, the new F 1 s peak (688.6 eV) and S 2p peak (162.4 eV) appear in the survey spectrum of FAgC@*p*-SF [34], and the C 1 s spectrum displays five resolved peaks of CH_2–CH_2 (284.8 eV), C═N (286.4 eV), C═O (288.6 eV), CF_2–CF_2 (291.8 eV), CF_2–CF_3 (293.7 eV) (Fig. S4) [27], indicating the successful modification of PFDT. Furthermore, the high-resolution Ag 3d peak of AgC@*p*-SF can be split into two peaks at 373.2 eV and 367.2 eV which are belonged to Ag $3d_{3/2}$ and Ag $3d_{5/2}$ (Fig. 2l), respectively, but the binding energy of them shift upward to 373.8 eV and 367.8 eV for FAgC@*p*-SF, verifying the interaction between AgNPs and PFDT and the formation of S-Ag bond [27]. Moreover, the deconvoluted S 2p spectrum in Fig. 2l clearly exhibits the peak of S $2p_{3/2}$ at 161.9 eV, S $2p_{1/2}$ at 163.8 eV, and the low coordination state of sulfur ions at 163 eV. And the peak at 164.3 eV further indicates the presence of typical metal–sulfur (M−S) bonds in the material [35].

Fig. 3 displays the sensing performances of the prepared FAgC@*p*-SF waterproof conductive fiber strain sensor. As illustrated in Fig. 3a, the in-situ recorded relative resistance variation ($\Delta R/R_0$, $\Delta R = R\text{-}R_0$, R and R_0 represent the resistance of the sensor under the stretching and initial state, respectively) of the FAgC@*p*-SF based strain sensors with different AgNPs loading under uniaxial tension were systematically investigated and compared. Clearly, $\Delta R/R_0$ of all sensors shows an exponential increasing trend with increasing strain, which can be ascribed to the gradually enhancement in the destruction of conduction paths upon external tension. Compared with the FC@*p*-SF based strain sensor with the absence of AgNPs, FAgC@*p*-SF based strain sensor displays a larger $\Delta R/R_0$ value under the same strain but a smaller sensing range, especially for the FAgC@*p*-SF with higher AgNPs loading. As a result, the strain sensing performance of FAgC@*p*-SF based strain sensor can be effectively tunned through simply changing the AgNPs loading.

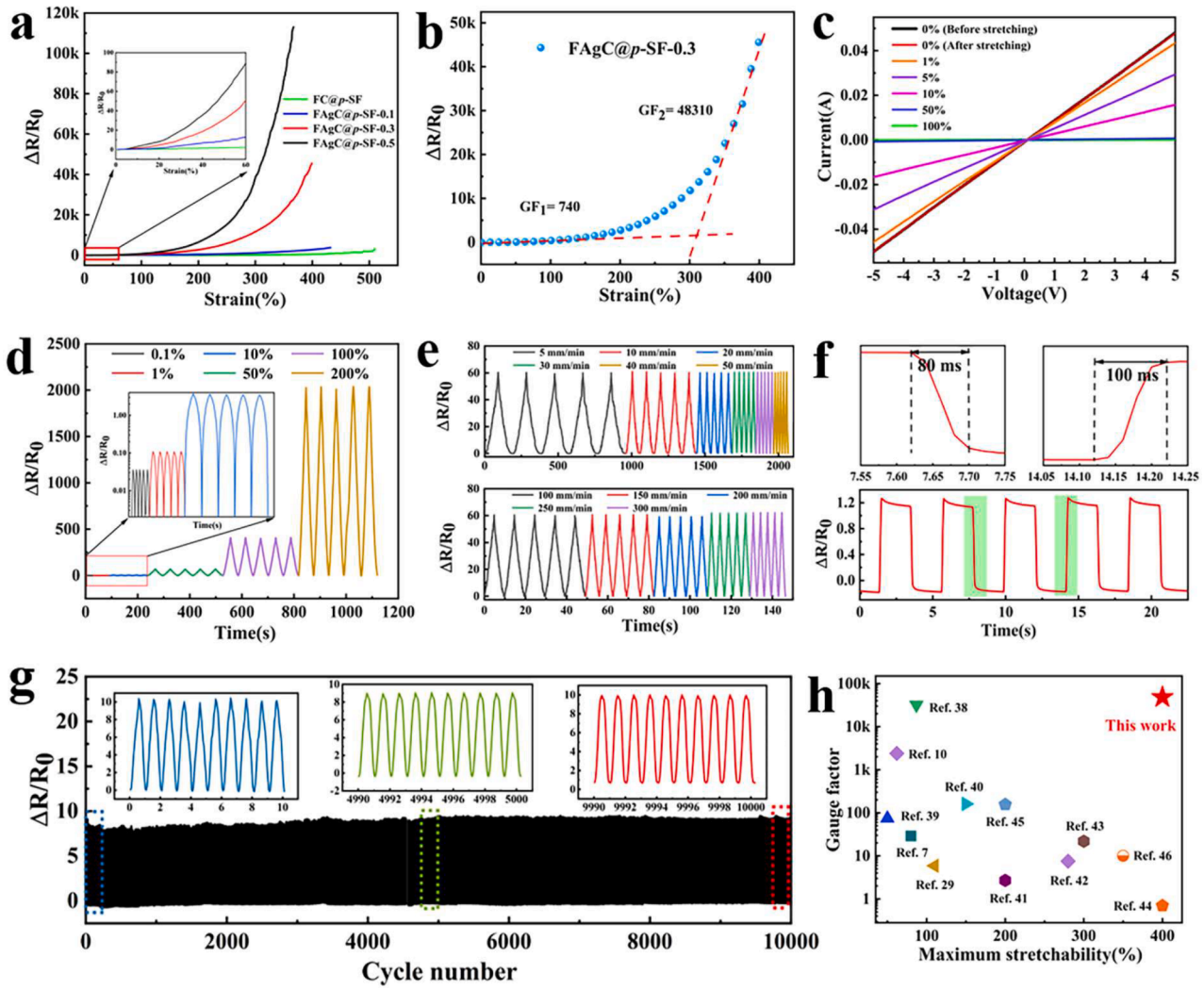

Fig. 3. Strain sensing performances of FAgC@*p*-SF waterproof conductive fiber strain sensor. (a) Relative resistance variation of different FAgC@*p*-SF based strain sensors as a function of strain. (b) Analysis on the strain sensitivity of FAgC@*p*-SF-0.3 based strain sensor. (c) I-V curves of FAgC@*p*-SF-0.3 based strain sensor under different strain amplitudes. Cyclic strain sensing behavior of FAgC@*p*-SF-0.3 based strain sensor under (d) different strain amplitudes at a strain rate of 10 mm/min and (e) different tensile rates at a 50% strain. (f) Response and recovery time of FAgC@*p*-SF-0.3 based strain sensor under 0.1% strain at a strain rate of 300 mm/min. (g) Long-term durability of FAgC@*p*-SF-0.3 based strain sensor over 10,000 cycles. (h) Comparation of the GF and maximum working range of our prepared FAgC@*p*-SF based strain sensor with other reported works.

Specifically, the maximum $\Delta R/R_0$ value of FC@*p*-SF, FAgC@*p*-SF-0.1, FAgC@*p*-SF-0.3, and FAgC@*p*-SF-0.5 is counted to be 3047, 3787, 45558, and 113000, and their corresponding maximum sensing range is 510%, 432%, 399%, and 367%, respectively. Here, the designed microcracked synergistic conductive layer can account for the typical AgNPs loading dependent strain sensing behavior, which will be systematically discussed in the following part.

After that, FAgC@*p*-SF-0.3 based strain sensor with both high $\Delta R/R_0$ and wide sensing range was selected for the detailed strain sensing performance study. Generally, gauge factor (GF= $(\Delta R/R_0)/\varepsilon$, ε represents the applied strain) is widely applied for evaluating the sensitivity of strain sensor. As seen in Fig. 3b, GF of the strain sensor is calculated to be -740 in the strain range of 0–150%, then it increases rapidly based on the slope of the $\Delta R/R_0$-strain curve and reaches a value up to 48,310 within the strain range of 335 to 400%, showing a persistent increase in sensitivity during the stretching process. It should be noted that the maximum GF is 18.5 times higher than that of FC@*p*-SF (GF = 2608 at 425 to 500% strain), demonstrating the prominent sensitivity enhancement effect of the synergistic conductive network. Fig. 3c displays the I-V curves of the sensor under different strain amplitudes, and the typical linear ohmic characteristic of them implies the good stability of the constructed conductive network upon external stretching. Besides, the slope of the I-V curve exhibits a decreasing trend with increasing strain amplitude, verifying the increase in resistance during the stretching process which is consistent with the results in Fig. 3b. Then, the I-V curve of the sensor after being released from a 100% strain can also be well coincided with its initial curve, illustrating the good recoverability of the conductive network that is beneficial for the cyclic stability of the sensor.

Cyclic strain sensing behavior of the sensor under different strain amplitudes and tensile rates are further studied. As seen in Fig. 3d, $\Delta R/R_0$ of the sensor exhibits a periodic increase and decrease towards cyclic stretching and releasing, and the maximum $\Delta R/R_0$ increases with increasing the strain amplitudes. Importantly, periodical sensing pattern with good stability and repeatability is well observed for the sensor under varying strain up to 200%, and an ultralow strain as low as 0.1% can also be accurately identified, which can be taken as the limit of detection of the sensor. Furthermore, it can be seen obviously from Fig. 3e that the sensor can also outputs stable and repeatable periodical sensing pattern with a constant response peak under various tensile rates ranging from 5 to 300 mm/min, showing the typical strain rate independent sensing capacity. All the results above indicate that the sensor

can effectively distinguish different strain levels without being disturbed by varying rates, demonstrating great promise for monitoring the irregular human body motions with varying movement amplitudes and frequencies.

Strain sensing behavior of the sensor towards a small (1% strain) and fast (300 mm/min) strain stimuli was conducted to investigate its response and recovery time. As displayed in Fig. 3f, $\Delta R/R_0$ of the sensor changes sharply once exerting and removing the strain, and the response time and recovery time are calculated to be 80 ms and 100 ms, respectively, showing a competitive advantage in detecting fast strain stimulus over other reported works [16,36–38]. To evaluate the long-term dynamic stability and durability of strain sensor in practical application, strain sensing performance of the sensor under 20% strain over 10,000 stretching and releasing cycles was studied, which displays stable sensing pattern with almost no obvious drift (Fig. 3g). What's more, as seen from the insets in Fig. 3g, the maximum $\Delta R/R_0$ keeps constant at a value of about 10, and the response curve maintains unchanged at different cycling periods, exhibiting excellent reproducibility and reliability. A comparation of sensitivity and working range between our prepared FAgC@*p*-SF based strain sensor with other reported works is shown in Fig. 3h, demonstrating the comprehensive advantages of our FAgC@*p*-SF based strain sensor which balances the trade-off between high sensitivity and wide working range successfully [7,10,29,38–46].

Subsequently, in-situ surface morphology observation of the prepared waterproof conductive fiber strain sensor under 200% strain was conducted to disclose the state of the synergistic CNTs and AgNPs conductive layer, which can be helpful to understand the detail strain sensing mechanism. As seen in Fig. 4a-c, amounts of small fragments appear in the upper conductive layer, and AgNPs hybrid with CNTs to constitute the lower conductive layer. As a result, a schematic illustration of the evolution of the designed microcracked synergistic conductive network during the stretching process was drawn and shown in Fig. 4d. In the initial state, it can be well known from Fig. 2 that the constructed conductive layer is mainly composed of lower stable synergistic AgNPs/CNTs conductive layer and upper tightly stacked AgNPs conductive layer, enabling the fiber with stable electrical property. When a small strain is applied, the lower entangled CNTs conductive network orients along the stretching direction without being destructed obviously, while lots of ultrasensitive microcracks are constructed on the surface due to the brittleness of the upper AgNPs layer, making the sensor to generate pronounced resistance change and high sensitivity. As the strain increases gradually, the microcrack propagates throughout the upper conductive layer, leading to the further increase in the number and width of microcrack, which is beneficial for a higher sensitivity. Meanwhile, the existence of AgNPs in the lower synergistic conductive layer can effectively reduce the winding degree of CNTs during the fabrication process, enabling it to be separated easily upon external stretching, contributing additional resistance change and improved sensitivity. Besides, the lower AgNPs/CNTs conductive network will also be completely destructed under a smaller strain compared with the pure CNTs networks, making the sensor display a decreased sensing range. As a result, a higher AgNPs loading can play a positive effect on the sensitivity of the sensor but a smaller strain sensing range. Thus, the prepared FAgC@*p*-SF exhibits a much higher sensitivity than that of FC@*p*-SF during the whole sensing range, which can be effectively tunned through changing the AgNPs loading.

Generally, waterproof surface can effectively improve the applicability of sensor in water or moisture environments. As seen in Fig. 5a & Video S2, the prepared FAgC@*p*-SF waterproof conductive fiber immersed into water displays a uniform silver-white "film" due to the trapped air layer on the surface induced total light reflection. Meanwhile, the incident water stream also bounces off the surface directly without leaving any trace (Fig. 5b & Video S3). Thus, it can be claimed that the water molecule can be effectively prevented from entering into the interior of conductive layer, avoiding the unstable signal output. As a proof of concept, strain sensing performance of the waterproof conductive fiber strain sensor immersed in water was continuously monitored, where the repeatable and recoverable response pattern is well maintained without any degradation even after 10 days (Fig. 5c), making it to be an ideal candidate for outdoor and underwater wearable electronic devices. Furthermore, as observed in Fig. 5d & Video S4, water droplet can roll on the surface of sample easily when moving the syringe needle, and there is no trace of water left after being pulled up, confirming the excellent non-adhesion property against water of the waterproof surface, which is beneficial for good self-cleaning property as a wearable device. Obviously, it can be seen from Fig. 5e & Video S5 that the muddy water rolls off the waterproof conductive fiber wound surface quickly, presenting sharp contrast to the common cotton fabric that absorb the muddy water easily. Besides, when dropping the common daily liquid foods (e.g., coffee, milk, tea, and milky tea) and different aqueous solution (e.g., acid solution, alkaline solution, and saline solution) on the wound surface, all the droplets still can always stay the spherical state without infiltrating into the surface, indicating the excellent self-cleaning and anti-corrosion property of our prepared FAgC@*p*-SF waterproof conductive fiber.

Here, the high sensitivity, wide working range, excellent reliability, and durability of the FAgC@*p*-SF waterproof conductive fiber strain sensor make it to be a competitive candidate for real time monitoring and discrimination of different human movement and physiological signals. As a proof of concept, the prepared waterproof conductive fiber

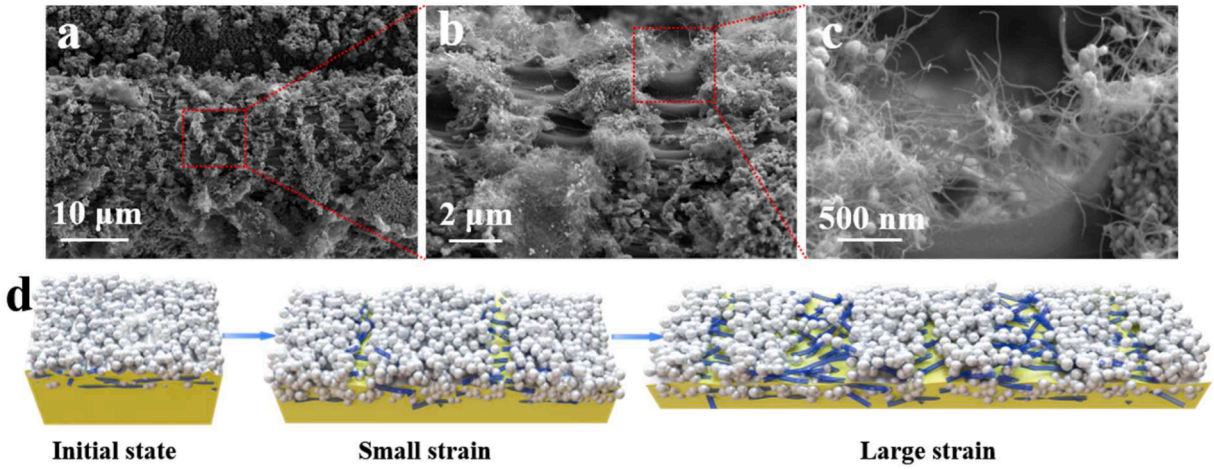

Fig. 4. (a-c) Surface SEM images of the FAgC@*p*-SF based strain sensor with different magnification under a 200% strain. (d) Schematic illustration of the evolution of the designed microcracked synergistic conductive network during the stretching process.

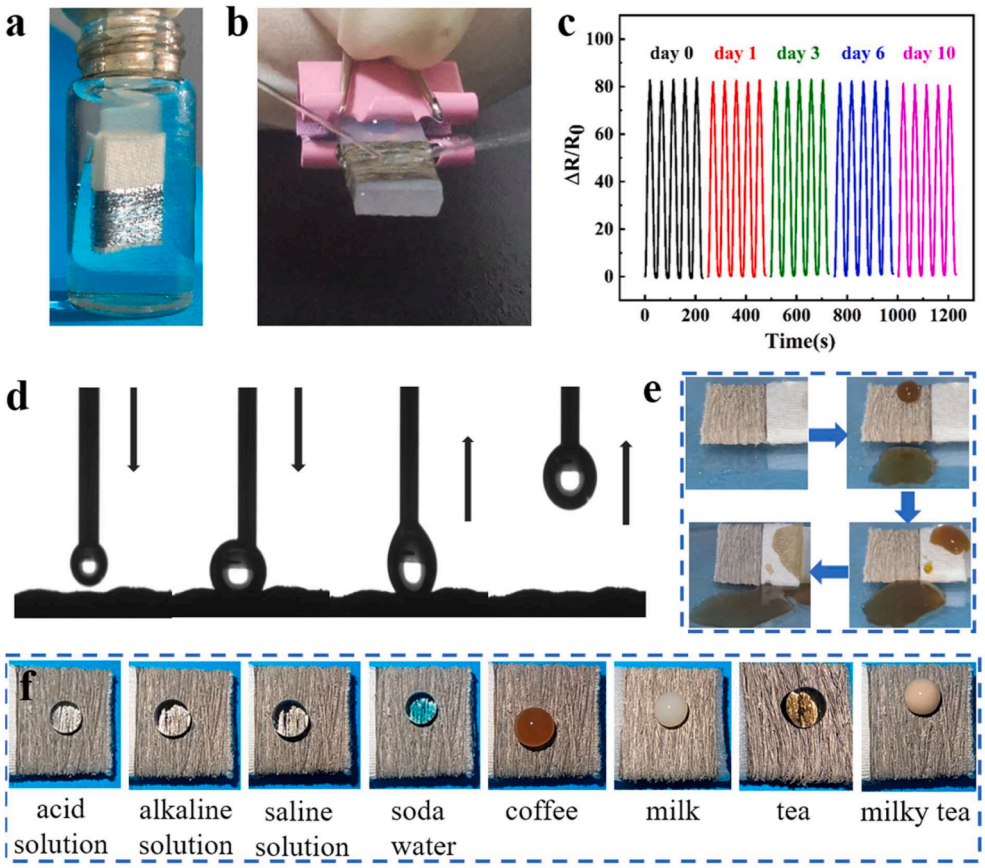

Fig. 5. Waterproof, self-cleaning, and anti-corrosion property of the FAgC@*p*-SF waterproof conductive fiber. Photograph showing (a) the strong light reflection of the waterproof fiber immersed in water and (b) the incident water stream bounces off the surface. (c) Strain sensing behavior of the sensor during a period of 10 days immersion in water. (d) Non-adhesion property of the waterproof surface. (e) Comparation of the self-cleaning property of the waterproof conductive fiber and cotton fabric. (f) Photograph showing the state of different droplets on the surface of waterproof conductive fiber.

was adhered onto different parts of human body to explore its promising application. As seen in Fig. 6a, the value of $\Delta R/R_0$ increases with flexing the wrist and then returns to its original value when the wrist is straightened, displaying the regular, periodic, and stable sensing signal. Meanwhile, the similar sensing pattern is also clearly observed for the human movements of finger bending and walking (Fig. 6b&c). Importantly, the sensing intensity of the sensor also shows an increasing trend with increasing the bending angle or walking frequency, demonstrating the excellent recognition towards different movements. Beyond that, the sensor was also applied for the detection of subtle physiological signals such as respiration and facial muscle motion. As shown in Fig. 6d, different respiratory states can be easily discriminated by the sensor attached onto the mask, where the normal breathing generates a low-intensity signal and the deep breathing generates a high-intensity signal. When fixing the sensor onto the cheek, the sensor outputs stable and reliable sensing signal when the volunteer smile that led to the stretching of facial muscles. But the grinning generates a stronger sensing intensity due to the increased stretching degree of facial muscles, displaying excellent distinguishability for different facial expression (Fig. 6e).

What's more, the excellent hydrophobic property of the sensor can effectively avoid the interference of water molecular that result in unstable sensing signal, enabling it to be applicable in various water environments. As seen in Fig. 6f, regular and stable sensing signals are acquired under different underwater finger bending modes, and the bending frequency can also be easily fixed based on the sensing pattern. Hence, the sensor possesses great promise for real-time monitoring and assessment of daily aquatic training of athletes. Finally, two sensors were symmetrically mounted onto the palmar side and dorsal side of wrist to explore its capacity for human gesture recognition. As depicted in Fig. 6g&h, both the two sensors adhered to the opposite locations output the same sensing signal when rotating the wrist because they suffered the same tension process. However, the two symmetric sensors output the complete contrary sensing pattern towards the downward bending of wrist due to the stretching and contraction of the palmar side and dorsal side of wrist. Conversely, the contrary sensing pattern is also observed for the upward bending of wrist. Thus, a reasonable layout of the sensor on any part of human body can achieve the human gesture recognition easily.

4. Conclusion

In summary, conductive spandex fiber with microcracked synergistic conductive layer was fabricated for wearable strain sensor *via* the simple solvent swelling and non-solvent-induced phase separation (NIPS) process, during which the in-situ reduced 0 dimensional AgNPs hybrid with one dimensional CNTs to construct the synergistic conductive network that can endow the sensor with wide working range and tunable sensing performances through changing the AgNPs loading. In addition, the outer AgNPs aggregation layer can be easily broken into amounts of small pieces, forming the ultrasensitive microcrack structure. Thus, the prepared strain sensor exhibits tunable and excellent overall sensing performances, such as high sensitivity (gauge factor is 48,310 within 335–400% strain), wide working range (0–400%), ultralow detection limit (0.1%), fast response/recovery time (80 ms/100 ms), and long-term fatigue resistance over 10,000 cycles. Furthermore, waterproof surface of the sensor was successfully obtained through modifying the outer microstructured AgNPs cluster with the low surface energy PFDT, exhibiting good corrosion resistance and self-cleaning properties. As a proof of concept, our prepared sensor can effectively detect both violent human movements and subtle physiological signals, and the good sensing capacity can also be well maintained in the humid and harsh underwater environments.

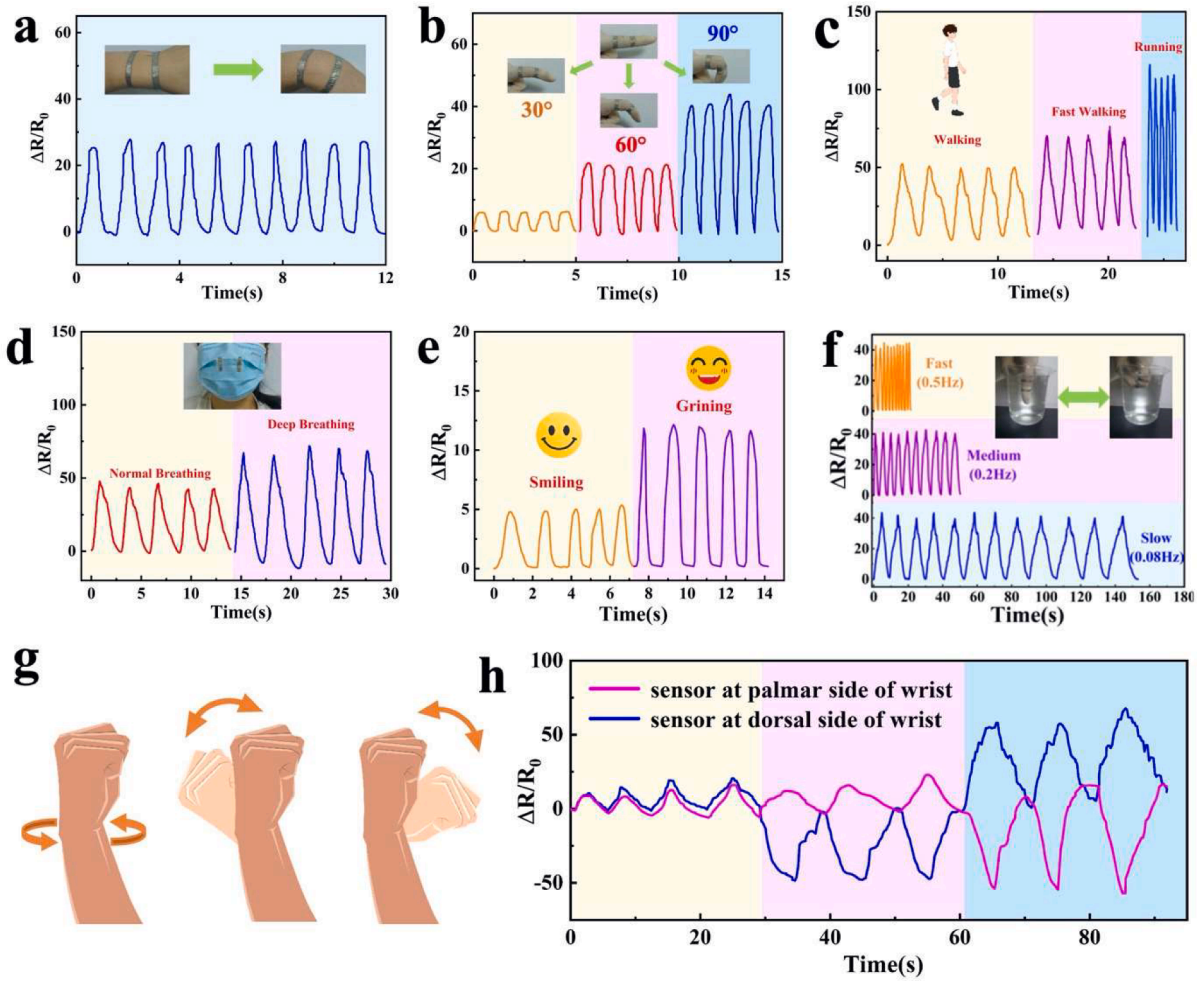

Fig. 6. Application of the FAgC@*p*-SF waterproof conductive fiber strain sensor for full-range human motion monitoring. Strain sensing performance of the sensor adhered to different body parts for the detection of (a) finger bending, (b) wrist flexing, (c) walking, (d) respiration, and (e) facial expression. (f) Underwater sensing stability investigation of the sensor under different finger bending modes. (g) Schematic diagram of wrist movement and (h) the corresponding sensing signals of two sensors adhered to the palmar side and dorsal side of wrist.

Declaration of Competing Interest

The authors declare that they have no known competing financial interests or personal relationships that could have appeared to influence the work reported in this paper.

Data availability

Data will be made available on request.

Acknowledgements

The authors gratefully acknowledge the financial support of this work by the National Natural Science Foundation of China (12072325), National Key R&D Program of China (2019YFA0706802), the 111 project (D18023).

Appendix A. Supplementary data

Supplementary data to this article can be found online at https://doi.org/10.1016/j.cej.2022.139716.

References

[1] W. Yang, H. Liu, C. Liu, C. Shen, Construction of skin-electrode mechanosensing structure for wearable and epidermal electronic sensor, Science Bulletin 67 (2022) 569–571.
[2] Y. Zheng, R. Yin, Y. Zhao, H. Liu, D. Zhang, X. Shi, B. Zhang, C. Liu, C. Shen, Conductive MXene/cotton fabric based pressure sensor with both high sensitivity and wide sensing range for human motion detection and E-skin, Chem. Eng. J. 420 (2021), 127720.
[3] Y. Guo, X. Wei, S. Gao, W. Yue, Y. Li, G. Shen, Recent advances in carbon material-based multifunctional sensors and their applications in electronic skin systems, Adv. Funct. Mater. 31 (2021) 2104288.
[4] Z. Liu, G. Wang, C. Ye, H. Sun, W. Pei, C. Wei, W. Dai, Z. Dou, Q. Sun, C.T. Lin, Y. Wang, H. Chen, G. Shen, An ultrasensitive contact lens sensor based on self-assembly graphene for continuous intraocular pressure monitoring, Adv. Funct. Mater. 31 (2021) 2010991.
[5] F.B. Kadumudi, M. Hasany, M.K. Pierchala, M. Jahanshahi, N. Taebnia, M. Mehrali, C.F. Mitu, M.A. Shahbazi, T.G. Zsurzsan, A. Knott, T.L. Andresen, A. Dolatshahi-Pirouz, The manufacture of unbreakable bionics via multifunctional and self-healing silk-graphene hydrogels, Adv Mater 33 (2021) e2100047.
[6] J.H. Lee, E. Kim, H. Zhang, H. Chen, H. Venkatesan, K.Y. Chan, J. Yang, X. Shen, J. Yang, S. Jeon, J.K. Kim, Rational design of all resistive multifunctional sensors with stimulus discriminability, Adv. Funct. Mater. 32 (2021) 2107570.
[7] Y. Cai, J. Shen, G. Ge, Y. Zhang, W. Jin, W. Huang, J. Shao, J. Yang, X. Dong, Stretchable Ti3C2Tx MXene/carbon nanotube composite based strain sensor with ultrahigh sensitivity and tunable sensing range, ACS Nano 12 (2018) 56–62.
[8] J. Lee, S. Shin, S. Lee, J. Song, S. Kang, H. Han, S. Kim, S. Kim, J. Seo, D. Kim, T. Lee, Highly sensitive multifilament fiber strain sensors with ultrabroad sensing range for textile electronics, ACS Nano 12 (2018) 4259–4268.
[9] C. Li, S. Yang, Y. Guo, H. Huang, H. Chen, X. Zuo, Z. Fan, H. Liang, L. Pan, Flexible, multi-functional sensor based on all-carbon sensing medium with low coupling for

ultrahigh-performance strain, temperature and humidity sensing, Chem. Eng. J. 426 (2021), 130364.
[10] C. Li, D. Zhang, C. Deng, P. Wang, Y. Hu, Y. Bin, Z. Fan, L. Pan, High performance strain sensor based on buckypaper for full-range detection of human motions, Nanoscale 10 (2018) 14966.
[11] H. Sun, Y. Bu, H. Liu, J. Wang, W. Yang, Q. Li, Z. Guo, C. Liu, C. Shen, Superhydrophobic conductive rubber band with synergistic dual conductive layer for wide-range sensitive strain sensor, Science Bulletin 67 (2022) 1669–1678.
[12] Y. Bu, T. Shen, W. Yang, S. Yang, Y. Zhao, H. Liu, Y. Zheng, C. Liu, C. Shen, Ultrasensitive strain sensor based on superhydrophobic microcracked conductive Ti3C2Tx MXene/paper for human-motion monitoring and E-skin, Science Bulletin 66 (2021) 1849–1857.
[13] R. Yin, S. Yang, Q. Li, S. Zhang, H. Liu, J. Han, C. Liu, C. Shen, Flexible conductive Ag nanowire/cellulose nanofibril hybrid nanopaper for strain and temperature sensing applications, Sci. Bull. 65 (2020) 899–908.
[14] Q. Li, R. Yin, D. Zhang, H. Liu, X. Chen, Y. Zheng, Z. Guo, C. Liu, C. Shen, Flexible conductive MXene/cellulose nanocrystal coated nonwoven fabrics for tunable wearable strain/pressure sensors, J. Mater. Chem. A 8 (2020) 21131–21141.
[15] H. Liu, Q. Li, Y. Bu, N. Zhang, C. Wang, C. Pan, L. Mi, Z. Guo, C. Liu, C. Shen, Stretchable conductive nonwoven fabrics with self-cleaning capability for tunable wearable strain sensor, Nano Energy 66 (2019), 104143.
[16] D. Zhang, R. Yin, Y. Zheng, Q. Li, H. Liu, C. Liu, C. Shen, Multifunctional MXene/CNTs based flexible electronic textile with excellent strain sensing, electromagnetic interference shielding and Joule heating performances, Chem. Eng. J. 438 (2022), 135587.
[17] L. Lin, Y. Choi, T. Chen, H. Kim, K.S. Lee, J. Kang, L. Lyu, J. Gao, Y. Piao, Superhydrophobic and wearable TPU based nanofiber strain sensor with outstanding sensitivity for high-quality body motion monitoring, Chem. Eng. J. 419 (2021), 129513.
[18] L. Li, Y. Zheng, E. Liu, X. Zhao, S. Yu, J. Wang, X. Han, F. Xu, Y. Cao, C. Lu, H. Gao, Stretchable and ultrasensitive strain sensor based on a bilayer wrinkle-microcracking mechanism, Chem. Eng. J. 437 (2022), 135399.
[19] H. Zhang, D. Liu, J.H. Lee, H. Chen, E. Kim, X. Shen, Q. Zheng, J. Yang, J.K. Kim, Anisotropic, wrinkled, and crack-bridging structure for ultrasensitive, highly selective multidirectional strain sensors, Nanomicro Lett. 13 (2021) 122.
[20] C. Liu, L. Pan, C. Deng, P. Wang, CNC–Al_2O_3–Ti: a new unit for micro scale strain sensing, RSC Adv. 6 (2016), 107683.
[21] C. Li, L. Pan, C. Deng, P. Wang, Y. Huang, H. Nasir, A flexible, ultra-sensitive strain sensor based on carbon nanocoil network fabricated by an electrophoretic method, Nanoscale 9 (2017) 9872.
[22] C. Li, L. Pan, C. Deng, T. Cong, P. Yin, Z. Wu, A highly sensitive and wide-range pressure sensor based on a carbon nanocoil network fabricated by an electrophoretic method, J. Mater. Chem. C 5 (2017) 11892.
[23] Y. Li, J. Jia, H. Yu, S. Wang, Z.Y. Jin, Y.H. Zhang, H.Z. Ma, K. Zhang, K. Ke, B. Yin, M.B. Yang, Macromolecule Relaxation Directed 3D Nanofiber Architecture in Stretchable Fibrous Mats for Wearable Multifunctional Sensors, ACS Appl Mater Interfaces 14 (2022) 15678–15686.
[24] L. Xu, S.R. Gutbrod, A.P. Bonifas, Y. Su, M.S. Sulkin, N. Lu, H.J. Chung, K.I. Jang, Z. Liu, M. Ying, C. Lu, R.C. Webb, J.S. Kim, J.I. Laughner, H. Cheng, Y. Liu, A. Ameen, J.W. Jeong, G.T. Kim, Y. Huang, I.R. Efimov, J.A. Rogers, 3D multifunctional integumentary membranes for spatiotemporal cardiac measurements and stimulation across the entire epicardium, Nat Commun 5 (2014) 3329.
[25] L. Wu, L. Wang, Z. Guo, J. Luo, H. Xue, J. Gao, Durable and Multifunctional Superhydrophobic Coatings with Excellent Joule Heating and Electromagnetic Interference Shielding Performance for Flexible Sensing Electronics, ACS Appl Mater Interfaces 11 (2019) 34338–34347.
[26] J. Gao, J. Luo, L. Wang, X. Huang, H. Wang, X. Song, M. Hu, L.-C. Tang, H. Xue, Flexible, superhydrophobic and highly conductive composite based on non-woven polypropylene fabric for electromagnetic interference shielding, Chem. Eng. J. 364 (2019) 493–502.
[27] L. Wang, H. Wang, X.-W. Huang, X. Song, M. Hu, L. Tang, H. Xue, J. Gao, Superhydrophobic and superelastic conductive rubber composite for wearable strain sensors with ultrahigh sensitivity and excellent anti-corrosion property, J. Mater. Chem. A 6 (2018) 24523–24533.
[28] G. Liu, J. Xiang, Q. Xia, K. Li, T. Lan, L. Yu, Superhydrophobic cotton gauze with durably antibacterial activity as skin wound dressing, Cellulose 26 (2018) 1383–1397.
[29] J. Gao, B. Li, X. Huang, L. Wang, L. Lin, H. Wang, H. Xue, Electrically conductive and fluorine free superhydrophobic strain sensors based on SiO2/graphene-decorated electrospun nanofibers for human motion monitoring, Chem. Eng. J. 373 (2019) 298–306.
[30] Y. Liu, X. Cao, J. Shi, B. Shen, J. Huang, J. Hu, Z. Chen, Y. Lai, A superhydrophobic TPU/CNTs@SiO2 coating with excellent mechanical durability and chemical stability for sustainable anti-fouling and anti-corrosion, Chem. Eng. J. 434 (2022), 134605.
[31] L. Wang, L. Wu, Y. Wang, J. Luo, H. Xue, J. Gao, Drop casting based superhydrophobic and electrically conductive coating for high performance strain sensing, Nano Mater. Sci. 4 (2022) 178–184.
[32] B. Niu, S. Yang, T. Hua, X. Tian, M. Koo, Facile fabrication of highly conductive, waterproof, and washable e-textiles for wearable applications, Nano Res. 14 (2020) 1043–1052.
[33] T. Belin, F. Epron, Characterization methods of carbon nanotubes: a review, Mater. Sci. Eng., B 119 (2005) 105–118.
[34] S. Zhang, X. Huang, D. Wang, W. Xiao, L. Huo, M. Zhao, L. Wang, J. Gao, Flexible and superhydrophobic composites with dual polymer nanofiber and carbon nanofiber network for high-performance chemical vapor sensing and oil/water separation, ACS Appl Mater Interfaces 12 (2020) 47076–47089.
[35] C. Ren, X. Jia, W. Zhang, D. Hou, Z. Xia, D. Huang, J. Hu, S. Chen, S. Gao, Hierarchical porous integrated Co1−xS/CoFe2O4@rGO nanoflowers fabricated via temperature-controlled in situ calcining sulfurization of multivariate CoFe-MOF-74@rGO for high-performance supercapacitor, Adv. Funct. Mater. 30 (2020) 2004519.
[36] M. Lin, Z. Zheng, L. Yang, M. Luo, L. Fu, B. Lin, C. Xu, A. High-Performance, Sensitive, wearable multifunctional sensor based on rubber/CNT for human motion and skin temperature detection, Adv. Mater. 34 (2022) 2107309.
[37] Y. Hu, T. Huang, H. Zhang, H. Lin, Y. Zhang, L. Ke, W. Cao, K. Hu, Y. Ding, X. Wang, K. Rui, J. Zhu, W. Huang, Ultrasensitive and wearable carbon hybrid fiber devices as robust intelligent sensors, ACS Appl. Mater Interfaces 13 (2021) 23905–23914.
[38] Y. Wang, J. Hao, Z. Huang, G. Zheng, K. Dai, C. Liu, C. Shen, Flexible electrically resistive-type strain sensors based on reduced graphene oxide-decorated electrospun polymer fibrous mats for human motion monitoring, Carbon 126 (2018) 360–371.
[39] S. Pan, Z. Liu, M. Wang, Y. Jiang, Y. Luo, C. Wan, D. Qi, C. Wang, X. Ge, X. Chen, Mechanocombinatorially screening sensitivity of stretchable strain sensors, Adv Mater 31 (2019) 1903130.
[40] Y.R. Jeong, H. Park, S.W. Jin, S.Y. Hong, S.-S. Lee, J.S. Ha, Highly stretchable and sensitive strain sensors using fragmentized graphene foam, Adv. Funct. Mater. 25 (2015) 4228–4236.
[41] Z. Liu, D. Qi, P. Guo, Y. Liu, B. Zhu, H. Yang, Y. Liu, B. Li, C. Zhang, J. Yu, B. Liedberg, X. Chen, Thickness-gradient films for high gauge factor stretchable strain sensors, Adv. Mater. 27 (2015) 6230–6237.
[42] S. Gong, D.T.H. Lai, B. Su, K.J. Si, Z. Ma, L.W. Yap, P. Guo, W. Cheng, Highly stretchy black gold E-skin nanopatches as highly sensitive wearable biomedical sensors, Adv. Electron. Mater. 1 (2015) 1400063.
[43] S.L. Wang, X. Xu, Z. Han, H. Li, Q. Wang, B. Yao, Highly stretchable liquid-metal based strain sensor with high sensitivity for human activity monitoring, Mater. Lett. 308 (2022), 131277.
[44] Z. Zeng, S. Yu, C. Guo, D. Lu, Z. Geng, D. Pei, Mxene reinforced supramolecular hydrogels with high strength, stretchability, and reliable conductivity for sensitive strain sensors, Macromol. Rapid Commun. 2200103 (2022).
[45] Y. Cheng, R. Wang, J. Sun, L. Gao, A stretchable and highly sensitive graphene-based fiber for sensing tensile strain, bending, and torsion, Adv Mater 27 (2015) 7365–7371.
[46] P. Wang, B. Sun, Y. Liang, H. Han, X. Fan, W. Wang, Z. Yang, A stretchable and super-robust graphene superhydrophobic composite for electromechanical sensor application, J. Mater. Chem. A 6 (2018) 10404–10410.